

Searching for a heavy Higgs boson via the $H \rightarrow l\nu jj$ decay mode at the CERN LHC

K. Iordanidis¹ and D. Zeppenfeld

Department of Physics, University of Wisconsin, Madison, WI 53706

and

¹*Lincoln Capital Management Co., Suite 2100, 200 S. Wacker Dr.,
Chicago, IL, 60606*

Abstract

The discovery of a heavy Higgs boson with mass up to $m_H = 1$ TeV at the CERN LHC is possible in the $H \rightarrow W^+W^- \rightarrow l\nu jj$ decay mode. The weak boson scattering signal and backgrounds from $t\bar{t}jj$ and from W +jets production are analyzed with parton level Monte Carlo programs which are built on full tree level amplitudes for all subprocesses. The use of double jet tagging and the reconstruction of the W invariant mass reduce the combined backgrounds to the same level as the Higgs signal. A central mini-jet veto, which distinguishes the different gluon radiation patterns of the hard processes, further improves the signal to background ratio to about 2.5:1, with a signal cross section of 1 fb. The jet energy asymmetry of the $W \rightarrow jj$ decay will give a clear signature of the longitudinal polarization of the W s in the final event sample.

I. INTRODUCTION

In the effort to determine the dynamics of the spontaneous breaking of the electroweak gauge symmetry, the discovery of the Higgs boson would be of prime importance. Detecting the Higgs boson is one of the biggest challenges for the CERN LHC [1,2], both for a perturbative scenario for the symmetry breaking sector, with a Higgs boson mass below the Z -boson pair production threshold, and also if some strong interaction dynamics should be responsible for $SU(2) \times U(1)$ breaking [3,4]. In both cases small signal rates, due to small usable decay branching fractions and/or small production rates, or large Standard Model (SM) backgrounds will have to be faced.

In order to isolate a Higgs signal one will have to utilize all its characteristics. In turn this requires a simulation of the expected SM backgrounds with a high degree of detail, in a region of phase space where little or no experimental input exists at present. This problem is particularly acute for the search of a very heavy Higgs boson, with a mass above ≈ 600 GeV. Here one will want to search for a Higgs resonance in the scattering of longitudinal weak bosons, or, more generally, one will look for some structure in the invariant mass distribution of the produced weak boson pairs in electroweak processes of the type $q_1 q_2 \rightarrow q_3 q_4 V_L V_L$ [4].

Numerous studies over the past several years have indicated that for the weak boson scattering signal to be identifiable, it is necessary to tag one or possibly two of the forward jets which arise from the scattered quarks [5–9]. A second characteristic of the weak boson scattering process is the lack of color exchange between the two incident quarks, which distinguishes it from typical background processes which proceed via the t -channel exchange of color octet gluons. These different color structures are expected to lead to a rapidity gap signature for the signal, either in terms of soft hadrons, at low luminosity [10,11] or in terms of mini-jets [12].

The small branching ratios of purely leptonic decays of the produced weak bosons can be overcome by studying the semi-leptonic modes, e.g. $H \rightarrow W^+ W^- \rightarrow l \nu j j$. Here large backgrounds from W +jets production put a premium on good W -mass reconstruction of the two decay jets, in a situation where the large W energy leads to a small separation of the two jets. An advantage of this decay mode is the observability of the $W \rightarrow j j$ decay angular distribution which may allow a measurement of the longitudinal W polarization of the signal.

Most of these points have been considered before. The detectability of the $H \rightarrow W^+ W^- \rightarrow l \nu j j$ signal with jet tagging techniques, for example, has been discussed in the ATLAS and CMS technical design reports [1,2]. However, these studies have been based on parton shower Monte Carlo programs and it is not clear how well these programs describe the high p_T jets associated with the decaying W . Also the color coherence effects which are at the basis of a rapidity gap trigger cannot be expected to be modeled correctly in these analyses.

In this paper we perform a complementary study, based on full QCD matrix elements of all subprocesses contributing to the signal and to the various backgrounds. We consider the signal process [7,13,14]

$$q_1 q_2 \rightarrow q_3 q_4 W^+ W^- \rightarrow q_3 q_4 l \nu j j \quad (1)$$

(and crossing related ones) with a double forward jet tag on the two scattered quarks, q_3 and q_4 . For the dominant W +jets QCD background we thus need the QCD matrix elements for all subprocesses leading to $W + 4$ jet events [15,16]. Similarly, the potentially large $t\bar{t} \rightarrow bW^+ \bar{b}W^-$ background needs to be simulated with two additional partons in the final state [17], in order to account for the two tagging jets. When studying the consequences of different color structures

on soft gluon radiation patterns, the $\mathcal{O}(\alpha_s)$ QCD corrections for the signal must be known as well [18]. While the parton level Monte Carlo programs for the individual subprocesses have been available in the literature, we here perform a first study of the $H \rightarrow W^+W^- \rightarrow l\nu jj$ mode with full QCD matrix elements for signal and background subprocesses.

In Section II we present these calculational tools in some detail. For the discussion of gluon radiation patterns we employ the truncated shower approximation which is briefly described at the end of that section. The isolation of the $H \rightarrow W^+W^- \rightarrow l\nu jj$ signal, with double forward jet tagging, but without considering the W -mass reconstruction from the $W \rightarrow jj$ decay is considered in Section III. Here the hadronic system arising from the W -decay will be considered as a single jet. The properties of this W -decay jet, its internal dijet structure, and the measurement of the W -mass is the subject of Section IV. Here we also consider the measurement of the W polarization via the energy asymmetry of the two decay jets [6]. Parameterizing the results of the W -mass analysis in terms of a reconstruction efficiency, we return to the simpler analysis, without simulating the $W \rightarrow jj$ dijet structure, in Section V. We consider the mini-jet patterns which arise from additional gluon radiation in the Higgs signal and $W + 4$ jets background, or from b -quark jets in the $t\bar{t}$ background, as an additional selection criterion. With a central mini-jet veto above $p_{Tj} = 20$ GeV, the combined background is reduced well below the signal level, without significantly reducing the signal cross section. For an integrated luminosity of 100 fb^{-1} , the expected event rate after all cuts is 99 (91) events for a $m_H = 800$ GeV (1 TeV) Higgs boson signal, with a combined background of 41 events. These results suggest that the search for the Higgs boson at the CERN LHC can be extended to the 1 TeV region, in the semi-leptonic Higgs decay channel. Finally, a summary and our conclusions are given in Section VI.

II. CROSS SECTION CALCULATION FOR SIGNAL AND BACKGROUND

The signal process to be considered at lowest order is the subprocess

$$q_1q_2 \rightarrow q_3q_4W(\rightarrow l\nu)W(\rightarrow jj) \quad (2)$$

and crossing related processes. In the following we require double forward jet tagging (of the jets corresponding to quarks q_3 and q_4) and the presence of at least one additional high transverse momentum central jet (from $W \rightarrow jj$). These requirements are sufficient to eliminate soft and collinear divergences and they justify a few approximations in the cross section evaluations which will be discussed shortly.

All cross section calculations are performed numerically, for pp collisions at a center of mass energy $\sqrt{s} = 14$ TeV. Individual subprocess cross sections are determined by numerically evaluating polarization amplitudes, mostly by using the amplitude techniques of Ref. [19]. Even though this formalism is well suited to handle massive fermions, all quarks and W -decay leptons are treated in the massless approximation, except for the top-quarks. This approximation greatly speeds up the calculations. Consistent with it, no Cabibbo-Kobayashi-Maskawa mixing is included in the calculation, even for incoming quarks. The error introduced by this approximation is well below 5% and, hence, negligible compared to the typical uncertainties of a tree level calculation. W decays are evaluated in the zero-width approximation. However, the $W \rightarrow f\bar{f}'$ decay amplitudes are fully implemented and, thus, all correlations between the decay fermions are included in our calculation. Finally, the phase space integrals are performed with the adaptive

Monte Carlo integration routine VEGAS [20]. The statistical error of all Monte Carlo integrals is below 1%, except for the $W + 4$ jets process for which the statistical error on total cross sections is $\approx 1.5\%$.

In all calculations, input parameters are a Z -mass of $m_Z = 91.19$ GeV, $\sin^2 \theta_W = 0.231$ for the weak mixing angle, and $\alpha = 1/128.75$ for the QED fine-structure constant at the electroweak scale. From these $m_W = 79.9$ GeV is derived at tree level. The 1-loop formula is used for the strong coupling constant $\alpha_s(\mu_R^2)$, with $\alpha_s(M_Z^2) = 0.12$. For all processes, the MRS A parameterization of parton distribution functions is used [21,22]. Even though this parameterization is NLO and, hence, we are partially including higher order corrections, these ambiguities introduce negligible uncertainties. Finally, b -quark contributions to the initial state are neglected throughout.

In what follows, we give a brief account of calculational details for individual signal and background processes.

A. The Electroweak Process $qq \rightarrow qq(g)W^+W^-$

The signal process at leading order is $qq \rightarrow qqH \rightarrow qqW^+W^-$ with subsequent W -decay, i.e. emission of the Higgs boson off a t -channel W or Z as shown in Fig. 1(a). For a heavy Higgs boson mass ($m_H \gtrsim 600$ GeV) the narrow Higgs width approximation is no longer applicable and all weak boson scattering processes (like the ones shown in Fig. 1(b)) as well as W -bremsstrahlung off the quark lines (see Fig. 1(c)) must be considered [7,13,14]. In principle we need to evaluate the full set of $\mathcal{O}(\alpha_{ew}^4)$ diagrams for a W^+W^- final state, including contributions from $q\bar{q}$ annihilation graphs and fermion interchange graphs for identical quarks. We will be requiring a double forward jet tag, however, which puts the final state quarks into very different phase space regions and at large invariant mass. As a result, annihilation diagrams such as the one shown in Fig. 1(d) and the interchange of identical fermions have very small contributions [18]. They will be neglected in the following. Within these approximations the helicity amplitudes for all subprocesses are evaluated numerically, using the results of Ref. [14].

The signal cross section, as discussed above, contains contributions from non-resonant electroweak processes such as W bremsstrahlung off the quark lines. Such contributions are independent of the mechanism for electroweak symmetry breaking and must be subtracted in order to get an estimate of the Higgs boson signal cross section. We model this continuum electroweak background by computing the signal at $m_H = 100$ GeV. The actual signal cross section is then defined as the difference between the heavy Higgs and the $m_H = 100$ GeV results, $\sigma_{sig} = \sigma(m_H) - \sigma(m_H = 100 \text{ GeV})$.

In order to understand the characteristics of soft parton emission in the Higgs signal process, the $\mathcal{O}(\alpha_{ew}^4 \alpha_s)$ QCD corrections to the processes of Eq. (2) are needed. The full set of real emission diagrams leading to a $W^+W^- + 3$ parton final state was calculated in Ref. [18] and we here use their results. The subprocesses to be considered are

$$q_1 q_2 \rightarrow q_3 q_4 g W(\rightarrow l\nu)W(\rightarrow jj) \quad (3)$$

and all crossing related processes like, for example,

$$q_1 g \rightarrow \bar{q}_2 q_3 q_4 W(\rightarrow l\nu)W(\rightarrow jj) . \quad (4)$$

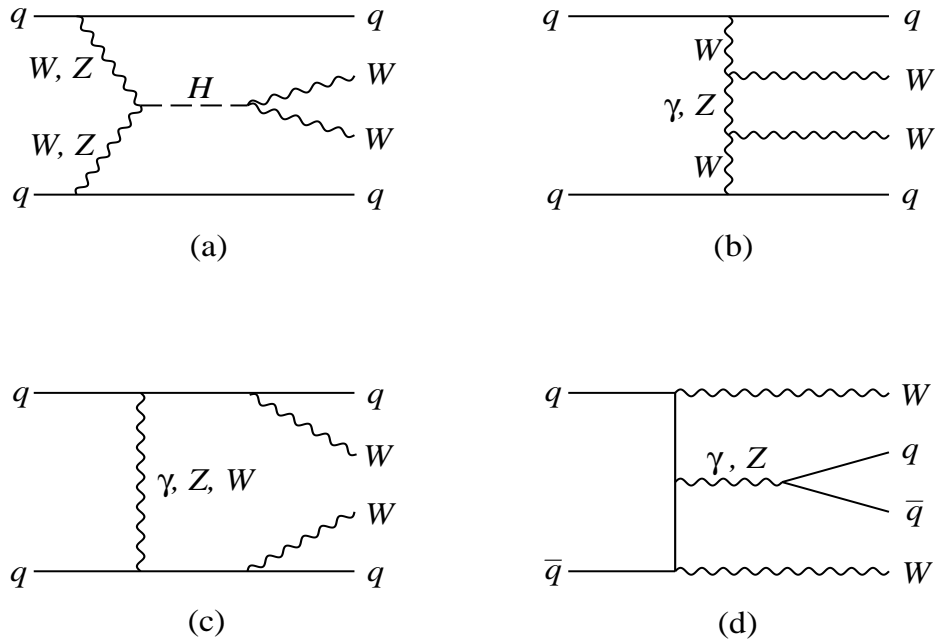


FIG. 1. Feynman diagrams for the electroweak processes $qq \rightarrow qqW^+W^-$. Representative graphs are shown for (a) Higgs boson production via weak boson fusion, (b) generic weak boson scattering, (c) W bremsstrahlung off the quark lines, and (d) quark-antiquark annihilation.

Again, s -channel graphs corresponding to $q\bar{q}$ -annihilation and Pauli interchange graphs for identical quarks are neglected. For the Higgs signal calculation at leading order and at $\mathcal{O}(\alpha_s)$ both the renormalization and the factorization scales are set to the smallest transverse momentum of the final state partons.

B. QCD W + Jets Background

In signal events with a high transverse momentum W which decays hadronically, $W \rightarrow q\bar{q}$, the two “jets” in the W decay may merge and form a single high p_T jet. In this case the signal events produce a $W + 3$ jets signature. The relevant QCD background for these events comes from QCD processes with a W and three jets in the final state. At leading order, two generic subprocesses contribute,

$$\begin{aligned}
 gg &\rightarrow q_1\bar{q}_2g W(\rightarrow l\nu) \\
 q_1\bar{q}_2 &\rightarrow q_3\bar{q}_4g W(\rightarrow l\nu).
 \end{aligned}
 \tag{5}$$

We use the results of Refs. [19,23] to calculate the cross sections for these events. All crossing related processes are included in the calculation.

When investigating questions like the W -invariant mass resolution in $W \rightarrow jj$ decays or the additional radiation of soft partons in $qq \rightarrow qqW^+W^-$ events, the QCD W + jets backgrounds with four partons in the final state are needed. The subprocesses that contribute can be classified as 6 quark processes, 4 quark plus 2 gluon processes, and 2 quark plus 4 gluon processes,

$$\begin{aligned}
q_1\bar{q}_2 &\rightarrow q_3\bar{q}_4q_5\bar{q}_6 & W(\rightarrow l\nu) \\
q_1\bar{q}_2 &\rightarrow q_3\bar{q}_4gg & W(\rightarrow l\nu) \\
gg &\rightarrow q_1\bar{q}_2gg & W(\rightarrow l\nu) .
\end{aligned} \tag{6}$$

The cross sections for these and all crossing related subprocesses were first calculated in Ref. [15]. Here we use equivalent matrix elements which were computed by generating the helicity amplitudes with the program MadGraph [16].

For the $W+n$ jets QCD processes the factorization scale is set equal to the smallest transverse momentum of the final state partons. At leading order these cross sections are proportional to α_s^n , and the strong coupling constant α_s is evaluated at the corresponding transverse momentum of each final state jet, i.e., $\alpha_s^n = \prod_{i=1}^n \alpha_s(p_{T,\text{jet}_i})$.

C. $t\bar{t}jj$ Background

For the $t\bar{t}$ background, the b -quarks from the $t \rightarrow Wb$ decay are produced mainly in the central region, with the two forward jets resulting mainly from QCD radiation. The relevant leading order process is the production of $t\bar{t}$ pairs in association with two jets, which includes the following subprocesses

$$\begin{aligned}
gg &\rightarrow t\bar{t}gg &\rightarrow W^+bW^-\bar{b} &gg \\
q\bar{q} &\rightarrow t\bar{t}gg &\rightarrow W^+bW^-\bar{b} &gg \\
q_1q_2 &\rightarrow t\bar{t}q_1q_2 &\rightarrow W^+bW^-\bar{b} &q_1q_2.
\end{aligned} \tag{7}$$

The exact matrix elements for the $\mathcal{O}(\alpha_s^4)$ processes are evaluated, including all the crossing related subprocesses. The Pauli interference terms between identical quark flavors in the process $q_1q_2 \rightarrow t\bar{t}q_1q_2$ are neglected, with little effect in the overall cross section rate, due to the large differences in the transverse momenta and energies of the final state partons [17]. The top quark decays are simulated in the narrow width approximation, and its mass is set to $m_t = 175$ GeV. The structure function scale is chosen to be the smallest transverse energy of the final state partons before the top quark decay. The strong coupling constant α_s is evaluated at the corresponding transverse energy of the final state partons, prior to the top quark decay, i.e., $\alpha_s^4 = \alpha_s(E_T(t))\alpha_s(E_T(\bar{t}))\alpha_s(p_{T,\text{jet}_1})\alpha_s(p_{T,\text{jet}_2})$.

In order to study the effects of additional parton radiation in the top quark background, one would like to evaluate the $t\bar{t} + 3$ jets cross sections as well. Since such a calculation is not available yet, we only consider the additional central jet activity arising from the b -quarks which are associated with the top-quark decays. The probability of a b -quark with $p_T^b > 20$ GeV to be identified as one of the two forward tagging jets was found to be small ($\approx 6\%$) [24]. With the transverse momentum and separation requirements on the two tagging jets to be discussed below, only this small fraction of the $t\bar{t}jj$ background is affected by collinear and infrared singularities. Instead of dropping these events altogether we regularize the singularities with the truncated shower approximation (TSA).

D. The Truncated Shower Approximation

As the transverse momentum of the softest parton becomes small, the perturbative calculation of the $\mathcal{O}(\alpha_s)$ cross section for both signal and background breaks down due to the collinear and

infrared divergences associated with gluon emission. In a complete next-to-leading order (NLO) calculation these divergences are eliminated due to the cancellation between virtual and real emission corrections. For the multi-parton processes considered here, a full NLO treatment is not yet possible, however. Instead, we model the effects of multiple soft gluon emission by using the truncated shower approximation (TSA) [25]. The TSA correctly reproduces the normalization of the lowest order cross section (which is free of infrared and collinear divergences) and it agrees with the full NLO calculation when the emission of one additional hard parton is considered. At the same time the TSA provides a model for the collective effects of multiple soft parton emission in events with n hard jets. Specifically, the tree level $n + 1$ -jet cross section is replaced by

$$\sigma(n + 1 j)_{TSA} = K \int f_{TSA}(p_{Tj,min}) \frac{d\sigma(n + 1 j)_{TL}}{dp_{Tj,min}} dp_{Tj,min} . \quad (8)$$

Here $p_{Tj,min}$ is the transverse momentum of the softest jet,

$$f_{TSA}(p_{Tj,min}) = 1 - \exp\left(-\frac{p_{Tj,min}^2}{p_{TSA}^2}\right) \quad (9)$$

is a Gaussian cutoff factor, and K is a multiplicative factor that effectively includes the full 1-loop corrections. It has been shown that the K -factor for vector boson scattering in pp collisions is small ($K = 1.06$ at the CERN LHC for $m_H = 800$ GeV) [26]. Since K -factors are unknown for the background processes we set $K = 1$ throughout this study. The parameter p_{TSA} is chosen so that the cross section of Eq. (8) correctly reproduces the lower order n jet cross section.

For jet transverse momenta $p_{Tj} < p_{TSA}$, the TSA leads to a reduction of the transverse momentum distribution of the hard n -jet system which simulates the canceling of multiple soft parton momenta. Thus p_{TSA} provides an estimate of the jet transverse momentum scale below which the emission of multiple soft gluons becomes important. In the phase space regions for hard jets to be discussed below, we find values of order $p_{TSA} \approx 40$ GeV for the $W + 4$ jets QCD background as compared to $p_{TSA} \approx 8$ GeV for the signal.

For the $t\bar{t}$ background we apply the TSA only to those events where one of the b -quarks arising from the top quark decays gives rise to at least one of the two forward tagging jets. In such events one of the two additional final state partons can be soft, and the cross section is enhanced in the region of the phase space where the transverse momentum of that jet is small. In order to avoid this singular behavior, the TSA is applied only to this fraction of events, with $p_{TSA}^{t\bar{t}} = 42$ GeV [12].

III. DECIPHERING THE HIGGS SIGNAL FROM BACKGROUND

The signal process $qq \rightarrow qqH \rightarrow qq(W \rightarrow l\nu)(W \rightarrow q\bar{q})$ gives rise to two forward tagging jets, one (or two) hard central jets from the hadronic W decay, and a leptonic W decay signature. In order for the W decay products to be identified, it is required that each event contains a charged lepton, l (either e or μ), in the central region, with

$$p_{Tl} > 100 \text{ GeV}, \quad |\eta_l| < 2, \quad \Delta R_{lj} = \sqrt{(\eta_l - \eta_j)^2 + (\phi_l - \phi_j)^2} > 0.7, \quad (10)$$

where p_{Tl} is the transverse momentum of the lepton, η_l is the lepton pseudo-rapidity, and ΔR_{lj} is the distance between the lepton and any identified jet in the pseudo-rapidity-azimuthal angle

plane. In addition, it is assumed that each event has large missing transverse momentum due to the neutrino of the $W \rightarrow l\nu$ decay,

$$p_T > 100 \text{ GeV} . \quad (11)$$

All final state partons are identified as jets if they satisfy

$$p_{Tj} > 20 \text{ GeV} , \quad |\eta_j| < 4.5 , \quad (12)$$

and if they are well separated in the pseudo-rapidity-azimuthal angle plane, with

$$\Delta R_{jj} = \sqrt{(\Delta\eta)^2 + (\Delta\phi)^2} > 0.7 . \quad (13)$$

The requirements of Eq. (12) are superseded by more stringent requirements for the tagging jets and for the Higgs decay products. The hadronically decaying W of the Higgs boson signal is identified by requiring the existence of a large transverse momentum jet in the central region,

$$p_{Tj}^c > 300 \text{ GeV} , \quad |\eta_j^c| < 2 . \quad (14)$$

The two quark jets in the process $qq \rightarrow qqH$ are tagged by requiring the presence of two additional jets, in the forward and backward regions, with

$$p_{Tj}^{tag1} > 50 \text{ GeV} , \quad 2 < |\eta_j^{tag1}| < 4.5 , \quad (15)$$

and

$$p_{Tj}^{tag2} > 30 \text{ GeV} , \quad \begin{cases} -4.5 < \eta_j^{tag2} < -2 & \text{if } \eta_j^{tag1} > 0 \\ 2 < \eta_j^{tag2} < 4.5 & \text{if } \eta_j^{tag1} < 0 \end{cases} . \quad (16)$$

The asymmetric transverse momentum requirement on the two tagging jets is motivated by the fact that one of the jets has substantially higher median p_T than the other, as shown in Fig. 2.

The resulting cross sections for the signal and the background are shown in the first column of Table I. The $W+3$ jets background is a factor of 20 larger than the signal, whereas the $t\bar{t}$ background is a factor of three larger. In contrast, the electroweak continuum background is strongly suppressed by double tagging, due to the fact that the rapidity distribution of the two tagging jets for the electroweak background peaks in the central region [27]. At this level it contributes only $\sim 10\%$ to the signal cross section.

For the $W+3$ jets cross section with the tagging requirements of Eqs. (15) and (16), it is important to ensure that it is a well defined hard scattering process for which a perturbative evaluation is reasonable. In order to investigate the effect of double tagging on the cross section, we computed the $W+1$ jet cross section with the single jet satisfying Eq. (14), and the $W+2$ jets cross section with the two jets satisfying Eqs. (14) and (15). The W -decay leptons must satisfy the cuts of Eqs. (10,11). The $W+1$ jet cross section is 2.16 pb, whereas the $W+2$ jets cross section is 0.57 pb. The corresponding reduction factors are 3.8 from $W+1$ jet to $W+2$ jets and 8.7 from $W+2$ jets to $W+3$ jets, respectively. These factors are typical for perturbative QCD processes with successively larger numbers of jets and lend credence to the use of perturbation theory in the evaluation of the QCD $W+n$ jets backgrounds.

The signal to background ratio can be further improved by utilizing differences in the tagging jet characteristics between signal and background. The two forward jets for the signal are

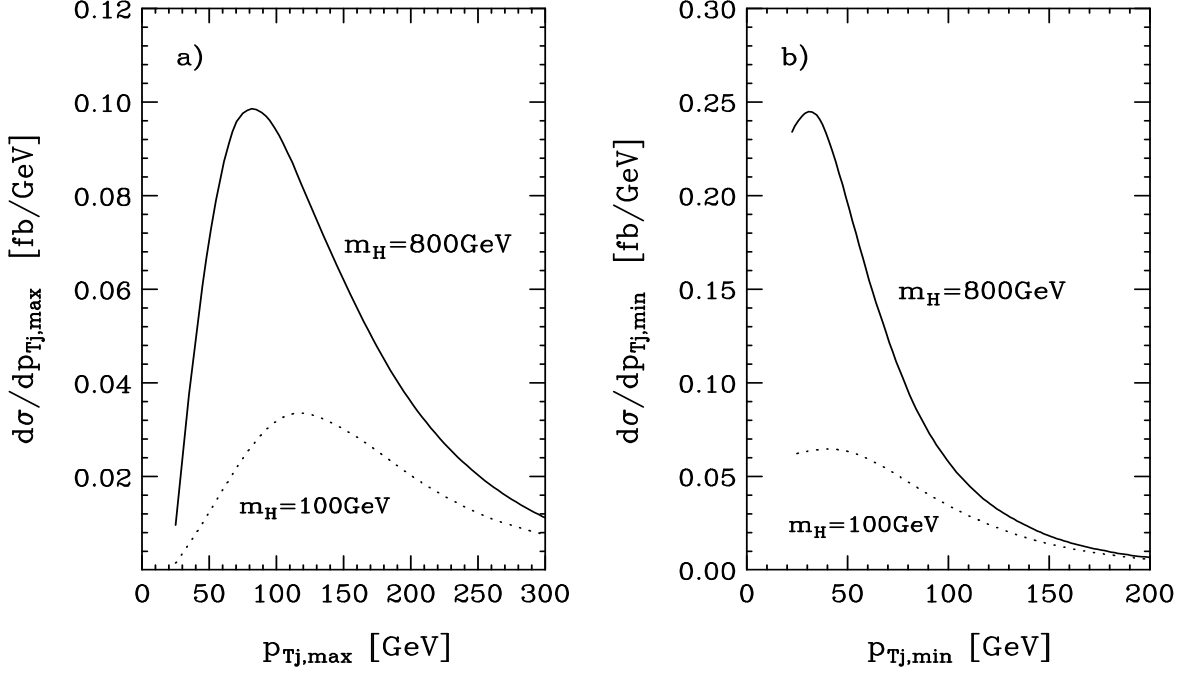


FIG. 2. Transverse momentum distributions (a) for the highest and (b) for the lowest p_T forward jets at $\sqrt{s} = 14$ TeV. For each event, a high transverse momentum lepton in the central region is required, $p_{Tl} > 100$ GeV and $|\eta_l| < 2$, as well as missing transverse momentum of $\cancel{p}_T > 100$ GeV. In addition a minimum of three visible jets are required, each with $p_T > 20$ GeV. The solid line represents the full signal calculation for $m_H = 800$ GeV, while the dotted line represents the continuum electroweak background ($m_H = 100$ GeV).

very energetic and their energy distributions decline slower than the energy distributions of the two forward jets for the $W+3$ jets and the $t\bar{t}jj$ backgrounds [8,9,24]. The softer jet energy distributions for the background reflect the fact that these jets tend to come from soft gluon radiation in the forward region. By requiring that both tagging jets satisfy

$$E_j^{tag1,2} > 500 \text{ GeV} , \quad (17)$$

the signal to background ratio can be improved by more than a factor of two (see second column of Table I). A second distinction arises in the pseudo-rapidity separation of the charged decay lepton and the closest tagging jet. For the Higgs signal there is little correlation between the two because the leptonic W -decay arises from the decay of a scalar particle which moves slowly in the laboratory frame. By contrast the $W + 3$ jets background contains many events with W bremsstrahlung off one of the tagging jets, and such events favor a small separation between the jet and the decay lepton. These differences are exploited by imposing a cut,

$$|\eta_j^{tag1,2} - \eta_l| > 2 , \quad (18)$$

on the separation between the decay lepton and the two tagging jets. The signal and background cross sections after all hard cuts are shown in the third column of Table I. The $W+3$ jets

TABLE I. Signal and background cross sections $B\sigma$ in fb after double jet tagging. The decay lepton acceptance requirements are $p_{T_l} > 100$ GeV and $|\eta_l| < 2$, and each event is required to have missing transverse momentum $\cancel{p}_T > 100$ GeV. The signal is defined as $\sigma(m_H) - \sigma(m_H = 100 \text{ GeV})$.

| | Double jet tagging [Eq.(14)-(16)] | +jet energy cut [Eq.(17)] | + lepton-tagging jet separation [Eq.(18)] |
|-------------------------|--------------------------------------|------------------------------|--|
| $m_H = 800 \text{ GeV}$ | 3.15 | 1.96 | 1.58 |
| $m_H = 100 \text{ GeV}$ | 0.26 | 0.18 | 0.10 |
| $W+3 \text{ jets}$ | 66.3 | 18.2 | 8.36 |
| $t\bar{t} + jj$ | 8.01 | 3.05 | 1.55 |
| <u>signal:</u> | | | |
| $m_H = 800 \text{ GeV}$ | 2.89 | 1.78 | 1.48 |

background is still a factor of 6 larger than the signal, whereas the $t\bar{t}$ background has been reduced to the same level as the signal.

We find that any further hardening of the acceptance criteria discussed so far will degrade the signal rate appreciably, with only marginal improvement to the signal's statistical significance. Additional information is needed in order to further suppress the background without significantly degrading the signal cross section. This is the focus of the following two sections.

IV. RECONSTRUCTION OF THE $W \rightarrow JJ$ DECAY

One additional piece of information is provided by the internal structure of the large transverse momentum jet in the central region which represents the hadronically decaying W of the Higgs signal. The invariant mass of this system, which may or may not be resolvable into two separate jets, provides an important criterion for suppressing the QCD W +jets background. Whenever the pair of jets from the hadronic W decay can be resolved, further information is gained. A Higgs boson decays mostly into longitudinally polarized W s whereas backgrounds with real W s are dominated by transversely polarized weak bosons. The angular distribution and the energy asymmetry of the two central jets are sensitive to the polarization of the W boson, and can be used in order to test whether or not the reconstructed W is the longitudinally polarized decay product of the Higgs boson [6,30].

Some of these questions have been studied previously with the aid of parton shower Monte Carlo programs [1,2,30,28]. Since we have a full QCD matrix element calculation available for the production of $W + 4$ jet events, we can avoid the approximations inherent in a parton shower program and use full tree level QCD to simulate the two forward jets as well as the two central jets which would fake the hadronically decaying W . The $t\bar{t}$ background is not included in this study of jet mass effects since, similar to the signal process, the observed central jet pair is the result of the decay of a real W boson, which, typically, is longitudinally polarized.

When using W mass reconstruction, the experimental resolution of the dijet mass is the limiting factor. In order to model these experimental errors, the lateral granularity of the detector

must be taken into account. Following the design specifications of the CMS detector [31], we divide the legoplot into cells of size

$$\Delta\eta\Delta\phi = 0.1 \times 0.1 . \quad (19)$$

The momentum vectors of the two central jets are then corrected to point to the center of the cell. This correction is applied to the Higgs signal and to the continuum electroweak background, but not to the $W+4$ jets background. For the former these smearing effects are important, due to the resonance in the dijet invariant mass spectrum at $m_{jj} = m_W$, while the background exhibits a fairly flat dijet mass spectrum which mitigates any smearing corrections. The finite energy resolution of electromagnetic and hadronic calorimeters affects both signal and background cross sections because energy and transverse momentum distributions are typically quite steep. These energy resolution effects are taken into account by Gaussian smearing of the overall energy scales of massless parton four-momenta, with relative energy uncertainties [31],

$$\frac{\Delta E_{em}}{E} = \frac{0.03}{\sqrt{E}} \otimes \frac{0.15}{E} \otimes 0.005 , \quad (20)$$

and

$$\frac{\Delta E_{had}}{E} = \begin{cases} \frac{0.8}{\sqrt{E}} \otimes \frac{1.0}{E} \otimes 0.03 & \text{when } |\eta_j| \leq 2.5 \\ \frac{1.0}{\sqrt{E}} \otimes \frac{3.0}{E} \otimes 0.05 & \text{when } 2.5 < |\eta_j| < 4.5 \end{cases} \quad (21)$$

Here ' \otimes ' means that the terms are added in quadrature. Energy smearing according to Eqs. (20,21) is applied to both the signal and the $W + 4$ jets background.

A. Resolution of Jet Pairs from $W \rightarrow q\bar{q}'$ Decay

The resolution of the two jets from $W \rightarrow q\bar{q}'$ decay depends on the angular separation,

$$\Delta R_{jj}^c = \sqrt{(\eta_{j1} - \eta_{j2})^2 + (\phi_{j1} - \phi_{j2})^2} , \quad (22)$$

of the two partons in the legoplot. Furthermore, in order to suppress the QCD $W + 4$ jets background, it is advantageous to raise the transverse momentum threshold for each of the two central jets above our nominal value of 20 GeV. For the study of W hadronic decay we thus require the existence of two central jets, with the following acceptance requirements which are added to the requirements of the previous section:

1. Each of the central jet candidates must have large transverse momentum and be in the central rapidity region,

$$p_{Tj}^c > 50 \text{ GeV}, \quad |\eta_j^c| < 2 . \quad (23)$$

All jets passing this criterion form candidate pairs for the hadronic W decay products.

2. For each candidate pair, the reconstructed W must have large transverse momentum, and it must lie in the hemisphere opposite to the lepton-neutrino pair,

$$p_T^{jj} > 300 \text{ GeV}, \quad |\phi_{jj} - \phi_{l\nu}| > 90^\circ, \quad (24)$$

where $\phi_{jj} - \phi_{l\nu}$ is the azimuthal angle between the jet-jet pair and the lepton-neutrino pair.

3. Finally, it is required that the two central jet candidates are separated by

$$0.2 < \Delta R_{jj}^c < 1.0. \quad (25)$$

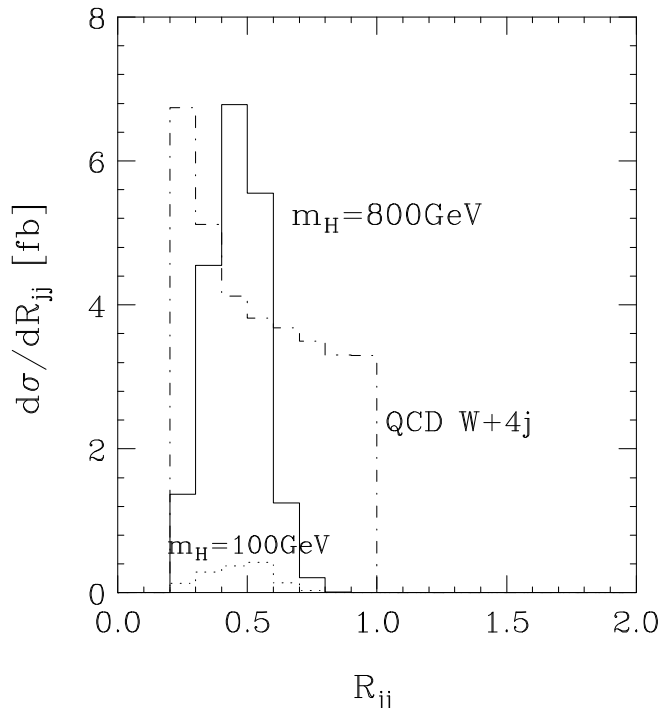


FIG. 3. Separation between the two central jets in the pseudo-rapidity-azimuthal angle plane. The solid histogram represents the full signal calculation for $m_H = 800$ GeV, which still contains the continuum electroweak background (dotted line), calculated in terms of the $m_H = 100$ GeV cross section. The QCD $W+4$ jets background is given by the dash-dotted histogram. Energy smearing according to Eqs. (20,21) is applied to signal and background processes. Finite detector granularity (see Eq. (19)) is taken into account for the electroweak processes.

The ΔR_{jj}^c distributions for the signal and the background are shown in Figure 3. The minimum ΔR_{jj}^c requirement of 0.2 is still sufficient to eliminate the final state collinear singularity of the $W+4$ jets cross section at $\Delta R_{jj}^c \rightarrow 0$. Notice also that the maximum separation cut, $\Delta R_{jj}^c < 1$, has an appreciable effect on the $W+4$ jets cross section only. Due to the large transverse momentum carried by the W (see Eq. (24)) and the associated strong boost of the W decay products, the two quarks from the W decay are rarely separated by more than $\Delta R_{jj}^c = 0.7$ in the laboratory frame.

TABLE II. Signal and background reduction factors resulting from an analysis of the central cluster which is a candidate for hadronic W decay. The first column gives the efficiency of reconstructing two jets in the central cluster, within the cuts of Eqs. (23–25). Requiring the invariant mass of these two jets to lie in the $M_W \pm 15$ GeV window yields the additional reduction factor of the second column. The product of the two yields the total efficiency listed in column three.

| | $\frac{\sigma(W \rightarrow jj)}{\sigma(W \rightarrow 1\text{jet})}$ [Eq. (19)–(25)] | $\frac{\sigma(W \rightarrow jj, M_{jj} \text{cut})}{\sigma(W \rightarrow jj)}$ [Eq. (26)] | Efficiency |
|-------------------|---|--|------------|
| $m_H = 800$ GeV | 0.87 | 0.83 | 0.71 |
| $m_H = 100$ GeV | 0.67 | 0.86 | 0.57 |
| $W + \text{jets}$ | 0.27 | 0.21 | 0.055 |
| <u>signal:</u> | | | |
| $m_H = 800$ GeV | 0.88 | 0.83 | 0.73 |

In the previous Section, no requirement was imposed on the internal structure of the central hard jet. Resolving it into two jets, corresponding to the $W \rightarrow q\bar{q}'$ decay, will lead to a reduced rate for the signal. The corresponding cross section reduction factors, after the cuts of Eqs. (23–25), are listed in the first column of Table II. For the electroweak processes, the effects of detector granularity and of energy smearing must be included also in the determination of the single jet cross sections which serve to normalize these reduction factors. For the signal cross section, 86.4% of the events pass the selection criteria. The reduction in the cross section comes mostly from the minimum p_T requirement of 50 GeV for each of the two central jets. Only two thirds of the electroweak continuum background survive the cuts.

The continuum $W + \text{jets}$ background is reduced by approximately a factor 4 when the resolution of the central jet into two hard jets of $p_T > 50$ GeV is required. This reduction is gratifying since it indicates that the use of perturbative QCD is still warranted, in spite of the small minimal separation of 0.2 for the two almost collinear partons which mimic the $W \rightarrow jj$ decay.

B. Reconstruction of the W Invariant Mass

A further reduction of the background is achieved by requiring that the two hard central jets are consistent in invariant mass with a hadronically decaying W -boson. The reconstructed invariant mass distribution of these two jets is shown in Fig. 4.

The distributions for the signal and the continuum background are narrow and peak at M_W . The distribution for the $W + 4$ jets background, on the other hand, is flat, reflecting the fact that in this case the jet pair is not the decay product of a real W boson. These differences are exploited by a simple invariant mass cut on the central dijet pair,

$$M_W - 15 \text{ GeV} < M_{jj}^c < M_W + 15 \text{ GeV} . \quad (26)$$

The chosen mass window of ± 15 GeV is motivated by the signal width in Fig. 4 and agrees with results of a more complete detector simulation [1,2]. The reduction factors for both the signal and the background, due to the dijet mass cut of Eq. (26), are given in the second column of

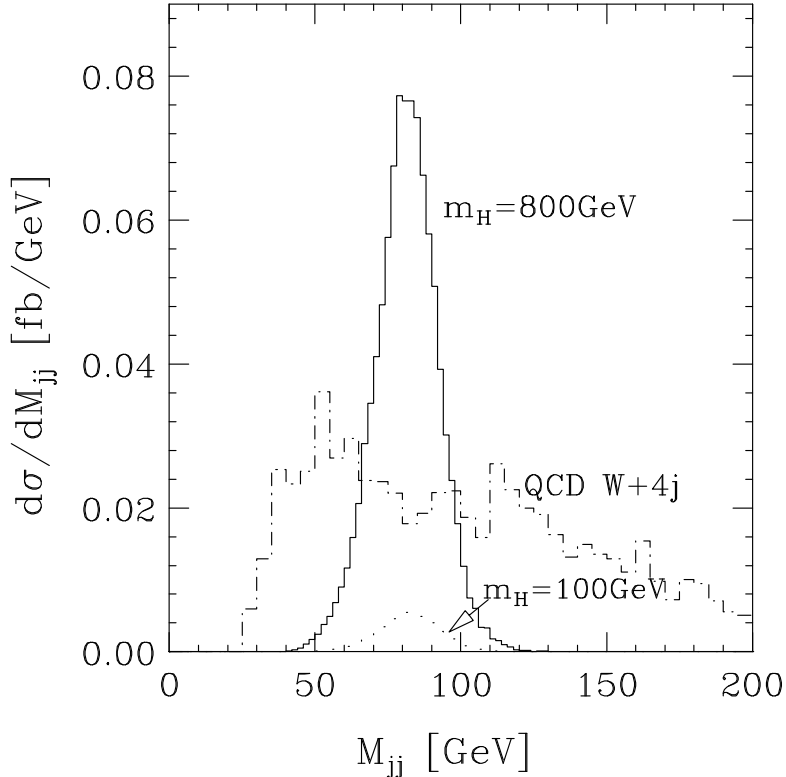


FIG. 4. Reconstructed dijet invariant mass distribution of the hadronically decaying W . The solid histogram represents the full signal calculation for $m_H = 800$ GeV, with the continuum electroweak background ($m_H = 100$ GeV) given by the dotted line. The QCD $W+4$ jets background is given by the dash-dotted histogram. Finite detector resolution is taken into account as in Fig. 3.

Table II. The $W+4$ jets background is reduced by an additional factor of 5, whereas 83% of the signal events survive the cut. The overall efficiency of the central jet resolution and the W invariant mass cut is given in the third column of Table II. For the Higgs boson signal, 73% of the events survive all cuts, in contrast to only 5.5% of the events for the $W+4$ jets background. At this level, the $W+4$ jets background is a factor of 2.3 smaller than the signal. Even if the central jet pair cannot be resolved, it may still be possible to measure the invariant mass of the broad central jet representing the hadronically decaying W boson. The reduction factors in the second column of Table II and the cross section values in the last column of Table I indicate that the W invariant mass cut would reduce the $W+$ jets background to the level of the signal.

C. Measurement of the W Polarization

Any polarization of the hadronically decaying W affects the angular distributions of the two W decay jets. A transversely polarized W yields a $1 + \cos^2\theta^*$ distribution whereas longitudinally polarized W s produce a $\sin^2\theta^*$ distribution. Here θ^* is the polar angle of one of the decay jets with respect to the W direction, in the W rest frame. The approximate alignment of the thrust axis with the W direction for transverse W s produces two jets of quite different energies after boosting into the laboratory frame. Longitudinally polarized W s, on the other hand lead to

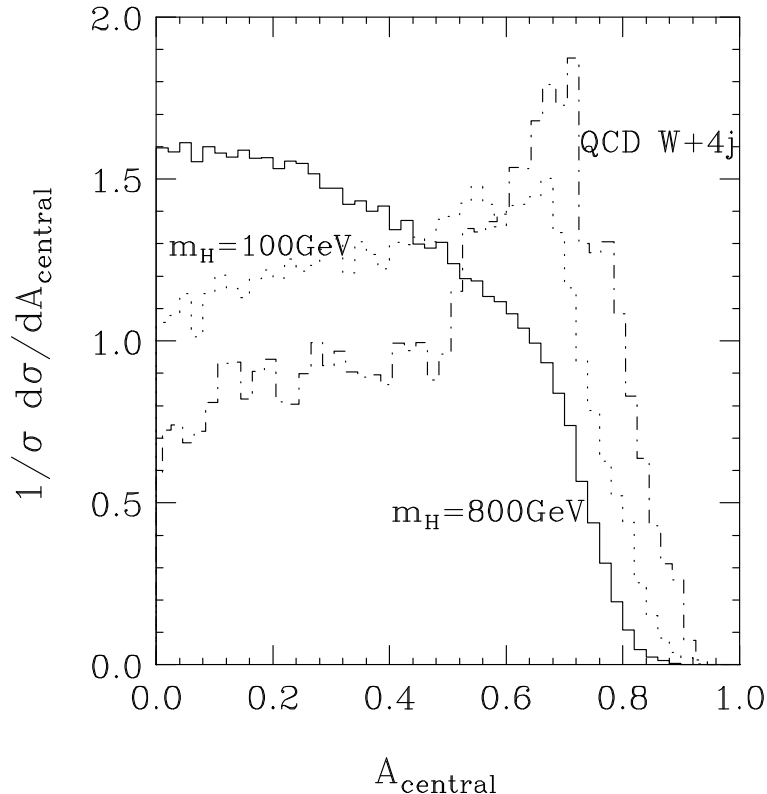


FIG. 5. Energy asymmetry distribution of the two central jets, which are identified as the $W \rightarrow jj$ decay products. No dijet invariant mass cut is imposed. The solid histogram represents the full signal calculation for $m_H = 800$ GeV, while the continuum electroweak background ($m_H = 100$ GeV) is given by the dotted line. The dash-dotted histogram represents the QCD $W+4$ jets background. Finite detector resolution is taken into account as in Fig. 3.

approximately equal jet energies. The energy asymmetry, A , of the two central jets therefore is an excellent variable to confirm the longitudinal polarization of the W s expected in Higgs boson decay [6]. It is defined as

$$A = \frac{|E_1 - E_2|}{E_1 + E_2} \quad (27)$$

where E_1 and E_2 are the energies of the two central jets in the laboratory frame. The energy asymmetry distributions for the $m_H = 800$ GeV signal and for the electroweak and the $W + 4$ jet QCD backgrounds are shown in Fig. 5, without imposing the dijet invariant mass cut of Eq. (26). Each distribution is normalized to the corresponding integrated cross section. The difference between the distributions for the signal and the background is striking. For the longitudinally polarized signal, the two jets have very similar energies so the distribution peaks at $A = 0$. In contrast, the two central jets of the $W + 4$ jets background and the two jets arising from the decay of a transversely polarized W in the electroweak continuum background have substantially different energies, with the distribution peaking at large values of A .

Clearly, an energy asymmetry cut (*e.g.* at $A = 0.5$) would further improve the signal to background ratio (by a factor of about 1.6). We do not impose such a cut here because there are other tools, namely a jet veto on the additional minijet activity in the central region, which can

be exploited for an adequate background rejection. The energy asymmetry can then be used to confirm the observation of longitudinally polarized W s from the Higgs boson decay.

V. CENTRAL JET VETO

In contrast to the $H \rightarrow W^+W^-$ signal, the two central W s will be accompanied by close-by b -quark jets in the $t\bar{t}jj$ background and, as we shall see, the W + jets QCD background also produces more observable central jets than the signal process. A veto on any *additional* central jet activity will thus substantially improve the signal to background ratio [14,12,1,2].

In order to study the effects of semi-soft parton radiation for the Higgs signal and the background, we use the TSA of Section IID, and thus we first need to estimate the TSA scales, p_{TSA} , for the various processes. For $W + 4$ parton production we find that $p_{TSA}^{W+4 jets} = 40.5$ GeV reproduces the $W + 3$ jets cross section of 8.36 pb in Table I. As discussed in Section IID we use $p_{TSA}^{t\bar{t}} = 42$ GeV for those $t\bar{t}jj$ events in which a b -quark arising in a top quark decay produces one of the forward tagging jets. For the Higgs signal, a separate estimate for the $m_H = 800$ GeV and $m_H = 100$ GeV cases gives two different values for p_{TSA} which, if used, will lead to an incomplete subtraction of the continuum electroweak background. Instead, we match the difference between the two cross sections, $B\sigma(m_H = 800 \text{ GeV}) - B\sigma(m_H = 100 \text{ GeV})$, to the lower order cross section, which gives $p_{TSA}^{H+3jets} = 7.9$ GeV.

The differences in p_{TSA} values between the signal and the background reflect the different characteristics of the corresponding hard scattering processes. For the signal, the momentum transfer, Q , to the color charges is given by the virtuality of the incident weak bosons in the longitudinal weak boson scattering process and, hence, $Q_{signal} \approx p_T^{\text{tag}} \lesssim M_W$. For the $W + 4$ jets and the $t\bar{t}$ backgrounds, on the other hand, the corresponding scales are substantially larger, of the order of $E_T(W)$ or, even, the partonic center of mass energy. Very roughly, p_{TSA} , the jet transverse momentum scale at which multiple parton emission becomes important, is one to two orders of magnitude smaller than the momentum transfer of the corresponding hard scattering process.

The signal and the background cross sections which are obtained within the TSA are given in the first column of Table III. Within the Monte Carlo errors they agree with the $W + 3$ jets, the $t\bar{t}jj$ and the signal cross sections in the last column of Table I. For all results presented in this section, the hadronically decaying W is again assumed to decay into a single observable jet. The resolution of this jet into two subjets and the effect of an invariant mass cut on this dijet system is then taken into account by multiplying with the efficiency factors given in Table II. Like the Higgs signal, the $t\bar{t}$ background contains a predominantly longitudinally polarized W which decays hadronically and the dijet resolution and dijet mass cut efficiencies for these decays will be similar to the ones found for the signal. The signal efficiency of 0.71 has therefore also been used for the $t\bar{t}$ background in the second column of Table III. This procedure gives a conservative estimate of the top quark background since the combinatorial dilution of the $W \rightarrow jj$ peak, due to b quarks misidentified as W decay jets, is not taken into account.

For the Higgs signal the two forward tagging jets define the phase space region in which to veto minijet activity. Color coherence favors additional parton emission outside the rapidity range bounded by the two tagging jets. A good way to capture the differences between the signal and the various backgrounds is by plotting the cross sections as a function of $\Delta\eta_{jj}$, the smallest relative distance, in units of pseudo-rapidity, between the extra jet and the two tagging jets,

TABLE III. Signal and background cross sections $B\sigma$ in fb, before and after the veto of additional central jets. Cuts in the first column are the same as in the last column of Table I, but cross sections are obtained within the TSA. The second column includes the dijet resolution and mass reconstruction efficiencies of Table II and columns three and four give cross sections and expected event rates after the central jet veto of Eq. (29). The Higgs signal cross section is defined as $B\sigma(m_H) - B\sigma(m_H = 100 \text{ GeV})$.

| | Hard cuts + soft jet (TSA) | + jj resolution and M_{jj} cut efficiency | + central jet veto | Number of events $\mathcal{L} = 100 \text{ fb}^{-1}$ |
|-------------------------|----------------------------------|---|-----------------------|---|
| $m_H = 800 \text{ GeV}$ | 1.64 | 1.17 | 1.07 | 107 |
| $m_H = 100 \text{ GeV}$ | 0.17 | 0.10 | 0.08 | 8 |
| $m_H = 1 \text{ TeV}$ | | | 0.99 | 99 |
| $W+4 \text{ jets}$ | 8.49 | 0.47 | 0.21 | 21 |
| $t\bar{t}$ | 1.55 | 1.10 | 0.12 | 12 |
| <u>signal:</u> | | | | |
| $m_H = 800 \text{ GeV}$ | 1.47 | 1.07 | 0.99 | 99 |
| $m_H = 1 \text{ TeV}$ | | | 0.91 | 91 |

$$\Delta\eta_{jj} = \text{sign} \left| \eta_j^{\text{tag}}(\text{closest}) - \eta_j^{\text{soft}} \right|. \quad (28)$$

Here $\eta_j^{\text{tag}}(\text{closest})$ is the pseudo-rapidity of the forward tagging jet which is closest to the soft jet. The sign in Eq. (28) is chosen such that $\Delta\eta_{jj}$ is negative if the additional jet is outside the pseudo-rapidity interval bounded by the two tagging jets and positive otherwise. The $\Delta\eta_{jj}$ distribution for additional jets with $p_{Tj} > 20 \text{ GeV}$ is shown in Figure 6. Both background distributions peak at $\Delta\eta_{jj} \sim 2$, indicating that the additional jet is predominantly emitted in the central region, between the two forward tagging jets. This is in contrast to the signal process, where an additional jet is emitted more forward than the tagging jets $\sim 50\%$ of the time. Because of the small scale governing gluon emission in the signal, only a small fraction of all signal events has an extra parton with transverse momentum in excess of 20 GeV. A good strategy is therefore to veto events with any additional jets between the two tagging jets, i.e. events which have an additional jet satisfying

$$p_{Tj}^{\text{soft}} > p_{T,\text{veto}} = 20\text{GeV}, \quad \eta_j^{\text{soft}} \in [\eta_j^{\text{tag1}}, \eta_j^{\text{tag2}}] \quad (29)$$

The rapidity requirement corresponds to a cut $\Delta\eta_{jj} > 0$ in Fig. 6.

The probability for finding a veto jet candidate depends strongly on the minimum transverse momentum, $p_{T,\text{veto}}$, of the additional jets. Within the TSA this probability can be estimated by integrating $d\sigma_{\text{TSA}}/dp_{Tj}^{\text{soft}}$ over the allowed p_{Tj} range. The result is then normalized to the lowest order cross section. Thus,

$$P(p_{Tj}^{\text{soft}} > p_{T,\text{veto}}) = \frac{1}{\sigma_{LO}} \int_{p_{T,\text{veto}}}^{\infty} \frac{d\sigma_{\text{TSA}}}{dp_{Tj}^{\text{soft}}} \cdot dp_{Tj}^{\text{soft}} \quad (30)$$

with $\eta_j^{\text{soft}} \in [\eta_j^{\text{tag1}}, \eta_j^{\text{tag2}}]$. This probability is shown in Figure 7. At $p_{T,\text{veto}} = 20 \text{ GeV}$, the probability for finding a veto jet candidate in a signal event is below 10%, whereas there is substantial

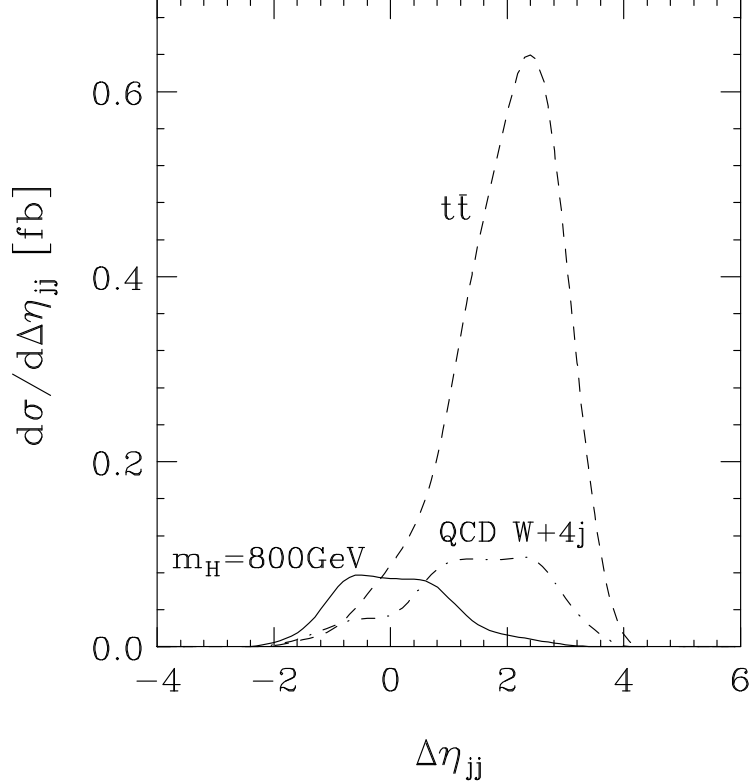


FIG. 6. Rapidity distance, $\Delta\eta_{jj}$, of secondary jets of $p_{Tj} > 20$ GeV from the closest forward tagging jet. Results are shown for the $m_H = 800$ GeV $\mathcal{O}(\alpha_s)$ electroweak processes (solid line), $t\bar{t}jj$ production (dash-dotted line) and QCD $W+4j$ production (dotted line). Negative values of $\Delta\eta_{jj}$ correspond to secondary jets outside the rapidity interval formed by the two forward tagging jets.

probability to find such a jet in background events ($\sim 55\%$ for the $W+4j$ jets and $\sim 90\%$ for the $t\bar{t}jj$ backgrounds). For the $t\bar{t}$ background, the veto probability tends to 1 as $p_{T,veto} \rightarrow 0$, due to the fact that one of the two b -jets is almost always emitted in the veto region. Within the TSA, the veto probability for the $W+4j$ jets background remains substantially less than 1, even if $p_{T,veto} \rightarrow 0$. This happens because in the TSA only one additional parton is emitted, with finite probability to be outside the veto region, as seen in Figure 6. Thus, at small $p_{T,veto}$ values, the TSA underestimates the veto probability.

An improved estimate of the veto probability at low $p_{T,veto}$ values is obtained by assuming that in the soft region multiple parton emission is dominated by the emission of gluons, and that the gluon emission probability exponentiates. This model of multiple minijet emission predicts a Poisson distribution for the multiplicity of additional minijets in hard scattering events. Indeed, recent CDF data are well described by this ansatz [32,33]. Within this exponentiation model, the veto probability can then be estimated as [12]

$$P_{exp}(p_{Tj}^{soft} > p_{T,veto}) = 1 - \exp\left[-\frac{1}{\sigma_{LO}} \int_{p_{T,veto}}^{\infty} \frac{d\sigma_{n+1}}{dp_{Tj}^{soft}} \cdot dp_{Tj}^{soft}\right] \quad (31)$$

where $d\sigma_{n+1}/dp_{Tj}^{soft}$ is the unregularized $n+1$ parton cross section, i.e. the higher order cross section without the truncated shower approximation.

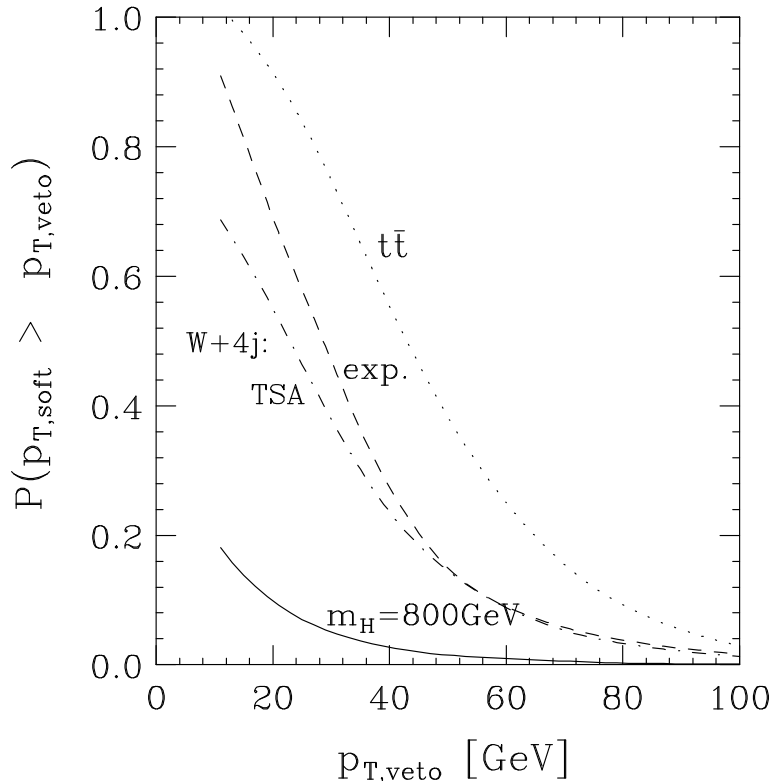


FIG. 7. Probability to find a veto jet candidate above a transverse momentum $p_{T,veto}$ between the two forward tagging jets. Results are derived in the TSA for the $m_H = 800$ GeV electroweak signal at $\mathcal{O}(\alpha_s)$ (solid line), $t\bar{t}jj$ production (dotted line) and QCD W +jets production (dash-dotted line). For QCD W +jets production the result for soft parton exponentiation is shown as the dashed line. See text for details.

A veto probability estimate based on Eq. (31) is also shown in Figure 7, for the $W+4$ jets background. At $p_{T,veto} = 20$ GeV, the TSA underestimates the veto probability by 20%. For large values of $p_{T,veto}$ ($p_{T,veto} > 50$ GeV), the two calculations give essentially the same veto probability. In the following estimates for the observability of a heavy Higgs signal at the LHC, the more conservative TSA results for the veto probability are used.

Signal and the background cross sections, after applying the central jet veto with $p_{Tj} > p_{T,veto} = 20$ GeV, are given in the third column of Table III. As expected, the jet veto is extremely effective in removing the $t\bar{t}$ background, due to the presence of the two b -jets. The integrated cross section is reduced by one order of magnitude and is now only $\sim 12\%$ of the signal cross section. The $W+4$ jets background is reduced by a factor 2.2. These background reductions are achieved with a very high efficiency for retaining the signal, with approximately 91% of the signal events passing the veto criterion.

After the veto of additional jets in the central region, the signal cross section rate is a factor of 2.5 larger than the combined background rate. Assuming an integrated luminosity of $\mathcal{L} = 100 \text{ fb}^{-1}$, the expected number of events for the Higgs signal and for the background are given in the last column of Table III. At $m_H = 800$ GeV, 99 signal events are expected with a total background of 41 events. These numbers indicate that the Higgs boson can be discovered

in the $H \rightarrow WW \rightarrow l\nu jj$ decay mode, for Higgs masses up to $m_H = 1$ TeV.

VI. DISCUSSION AND CONCLUSIONS

Our analysis of the $H \rightarrow WW \rightarrow l\nu jj$ decay mode of a heavy Higgs boson is based on complete tree level QCD calculations of the cross sections for the $qq \rightarrow qqWW$ signal as well as for the $W + 3, 4$ jets and $t\bar{t}jj$ background processes. Full QCD matrix elements provide the most reliable predictions for event features like hard jet distributions, the momentum scales governing the emission probability of additional soft jets, and the angular distributions of such additional jets. With QCD matrix elements for $(W \rightarrow l\nu)(W \rightarrow jj) + 2, 3$ jet events for the signal, $W + 3, 4$ jet events for the QCD background and $(t \rightarrow Wb)(\bar{t} \rightarrow W\bar{b}) + 2$ jet production for the top-quark background we have analyzed optimal criteria for double forward jet tagging, the expected resolution and expected background suppression when searching for a $W \rightarrow jj$ invariant mass peak, prospects for measuring the longitudinal polarization of the hadronically decaying W of the Higgs boson signal, and we have studied momentum scales and angular distributions of additional soft jet emission which would be affected by a central jet veto.

Previous analyses by the ATLAS [2] and CMS [1] Collaborations used parton shower programs like PYTHIA [34] instead, which give a more detailed description of other aspects of signal and background events, like particle content, higher soft jet multiplicities, and the presence of an underlying event. Carrying the simulation to the particle level also allows for a more realistic assessment of detector response. With fairly similar acceptance cuts on the Higgs decay products and using double forward jet tagging and central jet vetoing techniques these studies arrived at qualitatively the same answer: that a heavy Higgs boson can be discovered in the $H \rightarrow WW \rightarrow l\nu jj$ decay mode. It is reassuring that also quantitatively the agreement is excellent. The predicted rates for the Higgs boson signal and the various backgrounds found in the ATLAS and CMS analyses are somewhat smaller than ours, by up to a factor two. While this general trend is expected from including detector efficiencies, our central-jet-vetoing and forward-jet-tagging criteria differ sufficiently from those used in Refs. [1,2] that this agreement may be fortuitous to some extent. Since we do not have the parton level cross sections for these analyses, a more explicit and quantitative comparison with the ATLAS and CMS studies is not feasible. A few differences are noteworthy, however.

Both the CMS and the ATLAS analysis find suppression of the $W +$ jets background by a factor ≈ 3 from a central jet veto, but with very different values of $p_{T,veto} = 40$ GeV (CMS) and $p_{T,veto} = 15$ GeV (ATLAS), and ATLAS reports a decrease to a factor 2.5 when $p_{T,veto} = 40$ GeV is used, at high luminosity. Our analysis indicates that the veto probability should vary more strongly with $p_{T,veto}$ (see Fig. 7) and this question deserves further study. Another difference is the transverse energy requirement for the two tagging jets: our choice of transverse energy threshold for the tagging jets, $E_{T_j}(tag) > 50$ (30) GeV, is motivated by the signal distributions in Fig. 2. It is considerably harder than the values $E_{T_j}(tag) > 15$ GeV (ATLAS) and $E_{T_j}(tag) > 10$ GeV (CMS) used in the Technical Proposals of the two detectors [1,2]. Thus our choice definitely is conservative.

Neither of the presently available analyses will be definitive by the time the LHC experiments start taking data. The tools presented here, based on state-of-the-art QCD matrix elements, can be used to calibrate parton shower Monte Carlo programs. Combined with full detector

simulations they will provide the more reliable predictions for longitudinal weak boson scattering signals and background processes which are needed to understand LHC data.

ACKNOWLEDGMENTS

We are grateful to A. Stange for making his $t\bar{t}jj$ Monte Carlo program available to us and thank E. Mirkes for many useful conversations. This research was supported by the University of Wisconsin Research Committee with funds granted by the Wisconsin Alumni Research Foundation and by the U. S. Department of Energy under Grant No. DE-FG02-95ER40896.

REFERENCES

- [1] G. L. Bayatian *et al.*, CMS Technical Proposal, report CERN/LHCC/94-38 (1994).
- [2] W. W. Armstrong *et al.*, Atlas Technical Proposal, report CERN/LHCC/94-43 (1994).
- [3] J. F. Gunion, H. E. Haber, G.L. Kane, and S. Dawson, *The Higgs Hunter's Guide*, Addison-Wesley, 1990.
- [4] For recent reviews see e.g. J. Bagger *et al.*, *Phys. Rev.* **D49** (1994) 1246; *Phys. Rev.* **D52** (1995) 3878; M. E. Peskin, *Beyond the Standard Model*, Lectures given at *The 1996 European School of High-Energy Physics*, SLAC-PUB-7479 (1997) [hep-ph/9705479].
- [5] R. N. Cahn *et al.*, *Phys. Rev.* **D35**, 1626 (1987); V. Barger, T. Han, and R. J. N. Phillips, *Phys. Rev.* **D37** 2005 (1988).
- [6] R. Kleiss and W. J. Stirling, *Phys. Lett.* **200B**, 193 (1988).
- [7] U. Baur and E. W. N. Glover, *Nucl. Phys.* **B347**, 12 (1990); *Phys. Rev.* **D44**, 99 (1990).
- [8] D. Froideveaux, in *Proceedings of the ECFA Large Hadron Collider Workshop*, Aachen, Germany, 1990, edited by G. Jarlskog and D. Rein (CERN report 90-10, Geneva, Switzerland, 1990), Vol II, p. 444; M. H. Seymour, *ibid*, p. 557.
- [9] V. Barger *et al.*, *Phys. Rev.* **D44**, 1426 (1991).
- [10] Y. L. Dokshitzer, V. A. Khoze, and S. Troyan, in *Proceedings of the 6th International Conference on Physics in Collisions*, (1986) ed. M. Derrick (World Scientific, Singapore, 1987) p. 365.
- [11] J. D. Bjorken, *Int. J. Mod. Phys.* **A7**, 4189 (1992); *Phys. Rev.* **D47**, 101 (1993); J. D. Bjorken, in *Proceedings of the International Workshop on Photon-Photon Collisions*, (1992) ed. D. O. Caldwell and H. P. Paar (World Scientific, Singapore, 1992) p. 502.
- [12] V. Barger, R. J. N. Phillips, and D. Zeppenfeld, *Phys. Lett.* **B346**, 106 (1995) [hep-ph/9412276].
- [13] D. Dicus, J. F. Gunion, and R. Vega, *Phys. Rev. Lett.* **57**, 1110 (1986); *Phys. Rev.* **D37**, 2474 (1988).
- [14] V. Barger, K. Cheung, T. Han, and D. Zeppenfeld, *Phys. Rev.* **D44**, 2701 (1991); **48** 5444E (1993); **48**, 5433 (1993) [hep-ph/9305277].
- [15] F. A. Berends, H. Kuijf, B. Tausk, and W. T. Giele, *Nucl. Phys.* **B357**, 32 (1991).
- [16] T. J. Stelzer, and W. F. Long, *Comp. Phys. Comm.* **81**, 357 (1994); V. Barger, E. Mirkes, R. J. N. Phillips, and T. J. Stelzer, *Phys. Lett.* **B338**, 336 (1994).
- [17] A. Stange, private communication.
- [18] A. Duff and D. Zeppenfeld, *Phys. Rev.* **D50**, 3204 (1994).
- [19] K. Hagiwara and D. Zeppenfeld, *Nucl. Phys.* **B274**, 1 (1986); **B313**, 560 (1989).
- [20] G. Peter Lepage, *J. Comput. Phys.* **27**, 192 (1978).
- [21] A. D. Martin, R. G. Roberts, and W. J. Stirling, *Phys. Rev.* **D50**, 6734 (1994).
- [22] H. Plathow-Besch, *Int. J. Mod. Phys.* **A10**, 2901 (1995); H. Plathow-Besch, '*PDFLIB: Nucleon, Pion and Photon Parton Density Functions and α_s Calculations*', Users's Manual - Version 7.09, W5051 PDFLIB, 1997.07.02, CERN-PPE.
- [23] V. Barger, T. Han, J. Ohnemus, and D. Zeppenfeld, *Phys. Rev. Lett.* **62**, 1971 (1989); *Phys. Rev.* **D41**, 2782 (1989).
- [24] K. Iordanidis, PhD thesis, University of Wisconsin, Madison (1995).
- [25] V. Barger and R. J. N. Phillips, *Phys. Rev. Lett.* **55**, 2752 (1985); H. Baer, V. Barger, H. Goldberg, and R. J. N. Phillips, *Phys. Rev.* **D37**, 3152 (1988).
- [26] T. Han, G. Valencia, and S. Willenbrock, *Phys. Rev. Lett.* **69**, 3274 (1992);

- [27] U. Baur and E. W. N. Glover, Phys. Lett. **B252**, 683 (1990).
- [28] S. Abdullin, and N. Stepanov, CMS Technical Note CMS TN/94-178 (1994).
- [29] J. F. Gunion, Z. Kunszt, and M. Soldate, Phys. Lett. **B163**, 389 (1985); J. F. Gunion, and M. Soldate, Phys. Rev. **D34**, 826 (1986).
- [30] R. D. Field, and P. A. Griffin, Phys. Rev. **D48**, 3167 (1993); Phys. Rev. **D50**, 302 (1994).
- [31] CMS Collaboration, Letter of Intent, M. Markytan *et al.*, report CERN/LHCC 92-3 (1992).
- [32] CDF Collaboration, F. Abe *et al.*, Phys. Rev. Lett. **75**, 608 (1995).
- [33] D. Rainwater, D. Summers, and D. Zeppenfeld, Phys. Rev. **D55**, 5681 (1997).
- [34] H. U. Bengtsson and T. Sjostrand, Comput. Phys. Commun. **46** 43 (1987); T. Sjostrand, report LU-TP-95-20 (1995) [hep-ph/9508391].